Int. J. Electrochem. Sci., 8 **(2013)** 780 - 796

International Journal of ELECTROCHEMICAL SCIENCE
www.electrochemsci.org

Synthesis and Characterization of an Azo Dye: 4-(phenyldiazenyl)phenyl 2-furoate. Electrochemical and XPS Study of its Adsorption and Inhibitive Properties on Corrosion of Carbon Steel in Saline Water

Anca Moanta[1], *Adriana Samide*[1,*], *Catalina Ionescu*[1], *Bogdan Tutunaru*[1], *Aurelian Dobritescu*[1], *Alain Fruchier*[2], *Véronique Barragan-Montero*[3]

[1] University of Craiova, Faculty of Sciences, Calea Bucuresti 107 i, Craiova, Romania
[2] UMR CNRS 5253—ENSCM, 8 rue de l'Ecole Normale, 34296 Montpellier cedex 5, France
[3] Equipe SyGReM, Institut des Biomolécules Max Mousseron,'IBMM, UMR 5247, CNRS-UM1-UM2, ENSCM, 8, rue de l'Ecole Normale, 34296 Montpellier cedex 05, France
[*]E-mail: samide_adriana@yahoo.com

Received: 1 November 2012 / *Accepted:* 3 December 2012 / *Published:* 1 January 2013

The azo derivative namely 4-(phenyldiazenyl)phenyl 2-furoate (PPF), was obtained by an esterification reaction between 4-(phenyldiazenyl)phenol and 2-furoyl chloride in pyridine. The dye was characterized using elemental analysis, nuclear magnetic resonance (^{1}H and ^{13}C) and mass spectrometry with electro-spray ionization (ESI) techniques. The inhibitive properties of PPF on the corrosion of carbon steel in saline water (SW) have been investigated using potentiodynamic polarization, electrochemical impedance spectroscopy (EIS) and X-ray photoelectron spectroscopy (XPS). Electrochemical measurements showed that PPF acts as corrosion inhibitor of carbon steel in SW, by suppressing simultaneously the cathodic and anodic processes *via* adsorption on the carbon steel surface. The results indicated that an increase in the inhibitor concentration leads to an increase in both the charge-transfer resistance (R_{ct}) and inhibition efficiency (*IE*) and to a decrease of the corrosion current density (i_{corr}). Moreover, adsorption is spontaneous and is best described by Temkin isotherm. In the presence of PPF, XPS analysis confirmed the existence of a superficial layer providing a good corrosion protection of the electrodes. Parameterized Model number 3 (PM3) method was successfully used to predict the electron density distribution inside of PPF molecule.

Keywords: 4-(phenyldiazenyl)phenyl 2-furoate; chemical synthesis; adsorption and inhibitive properties; electrochemical measurements.

1. INTRODUCTION

Azo colourings are the most versatile class of dyes [1,2]. Their structure has been intensely studied and many spectral data analyses have already been reported [2,3]. The dyes have been most widely used in fields such as dying textile fibers, biomedical studies, advanced applications in organic synthesis and high technology areas like lasers, liquid crystalline displays, electro-optical devices and ink-jet printer [2-4]. The adsorption properties of different dyes were reported [5-7]. Organic dyes have also been reported as effective corrosion inhibitors of mild steel in different media [8-16]. Generally speaking, corrosion inhibitors reduce destructive attack initiated by physical, chemical and biological factors and which affects all materials used in various fields (e.g., mining, petroleum, oil sands and marine transportation). The corrosion protection efficiency of organic inhibitors depends on some physicochemical properties of the molecule (presence of O, N, S heteroatoms, functional groups, aromaticity, steric effects, electronic density), on the type of corrosive medium and nature of interaction between inhibitors and the vacant d-orbital of iron [17-21]. The inhibition performance of organic dyes was studied using weight loss and electrochemical measurements. The results showed that the dyes act as corrosion inhibitors by adsorption on the metal surface and that the inhibition efficiency increases with the increasing concentration of investigated dyes [8-16].

As part of our on-going interest on azo-derivatives and their chemical behaviour [22-26] we have prepared a new azo-dye, namely 4-(phenyldiazenyl)phenyl 2-furoate (PPF). In this study, we report the synthesis and characterization of PPF (elemental analysis, mass spectrometry, ^{1}H and ^{13}C NMR), as well as the results obtained in the investigation of the inhibitive properties of PPF for the corrosion of carbon steel in saline water (SW). In a previous study, we have reported the characterization of this compound using UV–Vis, FTIR, and thermal analysis. Moreover, its stability in different environments has been discussed [27].

2. EXPERIMENTAL

2.1. Synthesis

4-(phenyldiazenyl)phenol, pyridine and 2-furoyl chloride used in the synthesis were Aldrich products. 0.85 g (6.51 mmol) of 2-furoyl chloride were added to a solution formed by 1.3 g (6.56 mmol) of 4-(phenyldiazenyl)phenol in 30 mL of pyridine. The obtained solution was stirred for 60 minutes at room temperature and then left to stand overnight, after which it was poured over 100 mL of distilled water. 2 mL of concentrated HCl solution were then added and the mixture was filtered on a G_3 filter, the precipitate was washed with water and dried in the drying oven at 95 °C. The product was crystallized from ethanol to give PPF as a crystalline yellow powder, insoluble in water and stable in air at room temperature. Yield: 83%. R_f: 0.65 (toluene:acetone 9:1 V/V). The melting point was determined using a Boetius apparatus without correction: m.p.: 102 °C.

2.2. Characterization

2.2.1. Spectral studies

Elemental analysis of carbon, hydrogen and nitrogen has been performed using a Carlo-Erba O/EA 1108-analyzer. The mass spectrum obtained using electrospray ionization method (ESI) was realized on a Waters Micromass ZQ spectrometer using methanol as the solvent.

The NMR spectra were recorded at 20° C on a Bruker DRX-400 spectrometer working at 400.13 MHz for ^{1}H and 100.62 MHz for ^{13}C. The chemical shifts (δ) of ^{1}H and ^{13}C spectra are reported in ppm/TMS, with the ^{1}H $CHCl_3$ and ^{13}C $CDCl_3$ signals at 7.26 and 77.00 ppm respectively. The coupling constants (J) are reported in Hz. 1D spectra (^{1}H and ^{13}C-APT) and 2D spectra of homonuclear (COSYGP) and inverse heteronuclear (HMQCGP) correlations were recorded with the standard BRUKER sequences.

2.3. Corrosion tests

2.3.1. Materials

The used carbon steel had the following composition (% weight): C=0.1; Si=0.035; Mn=0.4; Cr=0.3; Ni=0.3, with the balance in Fe. The samples were mechanically polished with different grades of emery paper (down to 600), degreased with acetone and dried. All of the tests were performed in saline water (SW) containing 0.15 mol L^{-1} NaCl and 0.001 mol L^{-1} HCl (pH = 3) without PPF and with various concentrations of the dye.

2.3.2. Electrochemical measurements

Electrochemical measurements were performed using a Voltalab 40 model PGZ301 potentiostat/galvanostat driven by a personal computer with VoltaMaster 4 software. A typical three electrodes cell with a working electrode made of carbon steel with an active surface of 1 cm^2 was used. The auxiliary electrode was a platinum plate (1 cm^2) and the reference electrode was represented by a saturated Ag/AgCl electrode. Potentiodynamic polarization curves were obtained with the scan rate of 1 mV s^{-1}, in a potential range from -800 mV to -100 mV. The immersion time of the plates in the SW blank and in SW containing various concentrations of PPF was 30 minutes in open circuit at room temperature.

Electrochemical impedance spectroscopy (EIS) measurements were carried out after 30 minutes immersion time of the carbon steel plates in corrosive media, at the corrosion potential (E_{corr}), in a frequency range from 10^5 Hz to 10^{-1} Hz by a parturition signal of 10 mV amplitude peak to peak, at room temperature.

2.3.3. X-ray photoelectron spectroscopy (XPS)

X-ray photoelectron spectroscopy (XPS) spectra were recorded in a VG ESCA 3 Mk II-EUROSCAN spectrometer with a Mg K_ X-ray source (1486.7 eV photons energy) operated at 300 W (accelerating voltage 12.5 kV, emission current 24 mA). The pressure in the analysis chamber did not exceed the value of $2\text{-}3\cdot10^{-8}$ torr during all the period of spectra acquisitions. In order to perform the surface charge compensation, a FG40 flood gun device (Specs GmbH – Germany) has been used, with a 0.1 mA electronic current at a 2 eV energy. The samples were measured in an "as received" condition with no other surface cleaning treatment (chemical etching or Ar+ ion beam bombardment). Survey spectra were recorded with a window of 1200 eV and 100 eV pass energy. The Gaussian profile lines for curve fitting procedure was used. Binding energy calibration was done by linking the reference to C(1s) line, the binding of C-C or C-H located at 285 eV.

3. RESULTS AND DISCUSSION

3.1. Synthesis and characterization

PPF has been obtained using the reaction of 4-(phenyldiazenyl)phenol with 2-furoyl chloride in pyridine (Scheme 1). The composition and purity of the synthesized azo-ester was confirmed by elemental analysis. The obtained elemental analyses values for the compound $C_{17}H_{12}N_2O_3$ are the following: calculated: C, 69.86; H, 4.11; N, 9.59; found: C, 69.93; H, 4.16; N, 9.55.

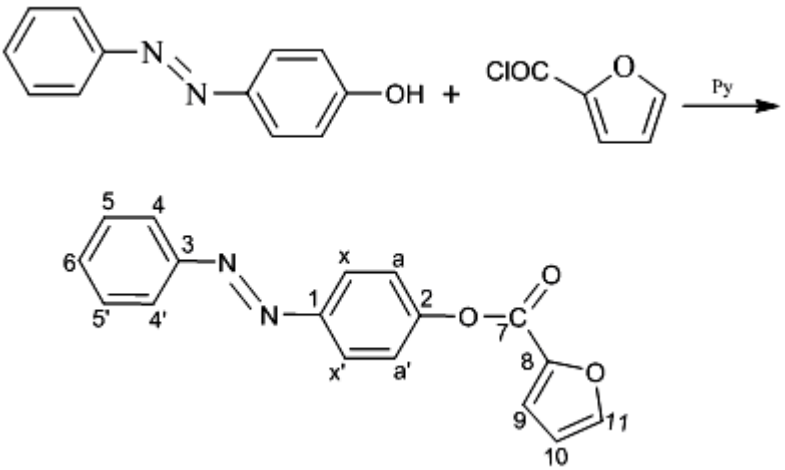

Scheme 1. 4-(phenyldiazenyl)phenyl 2-furoate (PPF) synthesis

The peaks that appear in the ESI^+ MS spectra of the investigated azoderivative (Fig. 1) are the corresponding adduct ion with sodium $[M+Na]^+$ at m/z 315, with a relative intensity of 100%, the protonated molecular ion $[M+H]^+$ at m/z 293 (RI=5.38%, Fig. 1, detail a), and the cluster ion $[2M+Na]^+$ at m/z 607 (RI=1.26, Fig. 1, detail b).

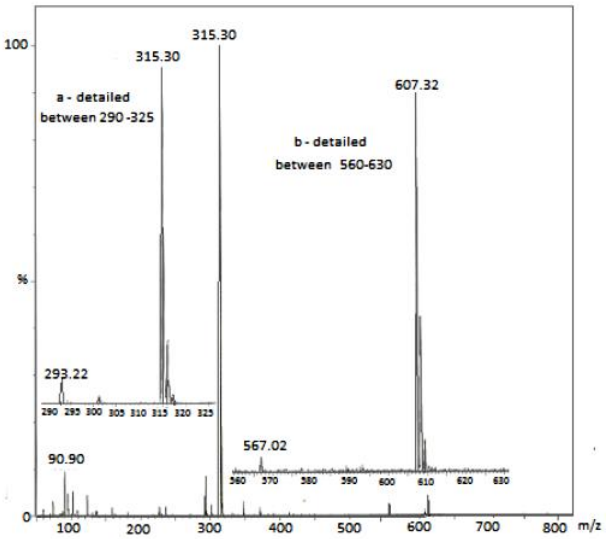

Figure 1. ESI mass spectrum of PPF. The description of the NMR spectra of the new dye is realized below.

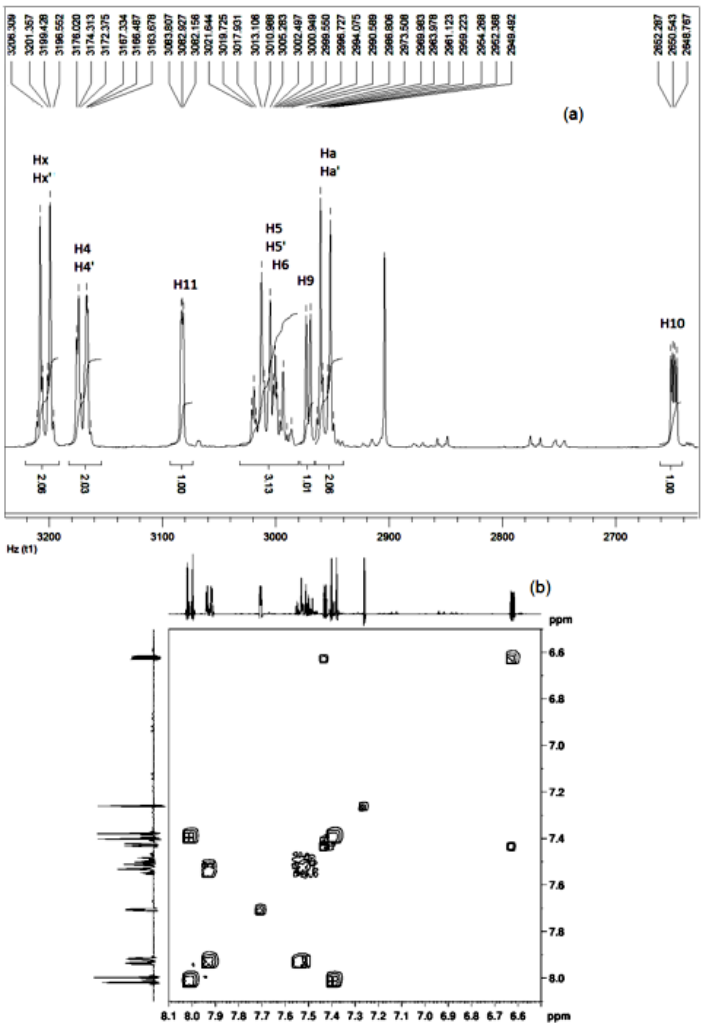

Figure 2. (a) ^{1}H NMR spectrum of PPF; (b) ^{1}H - ^{1}H correlation spectrum of PPF.

Fig. 2a shows that the signals of the four protons of the disubstituted aromatic ring form an AA'XX' system. The 2D COSY spectrum (Fig. 2b) shows that the two parts of this system are at 7.39 ppm and 8.01 ppm. Assuming that the substituent effects [28] of the two groups (R-N=N- and O-C(O)-R') are additive, signals at 7.39 and 8.01 ppm may be assigned to Haa' and Hxx' respectively. The signals of the monosubstituted aromatic ring protons are displayed as an AA'MM'P system at 7.92 ppm (H_4 and $H_{4'}$), 7.54 ppm (H_5, $H_{5'}$), and 7.48 ppm (H_6). On the other hand, H_9, H_{10} and H_{11} form double doublets at 7.43 ppm, 6.62 ppm and 7.70 ppm respectively.

The signals in ^{13}C NMR spectrum (Fig. 3a) have been assigned with the help of the 2D HMQC spectrum (Fig. 3b) and the substituent additive effects [29]. The results of these assignments are gathered in Table 1.

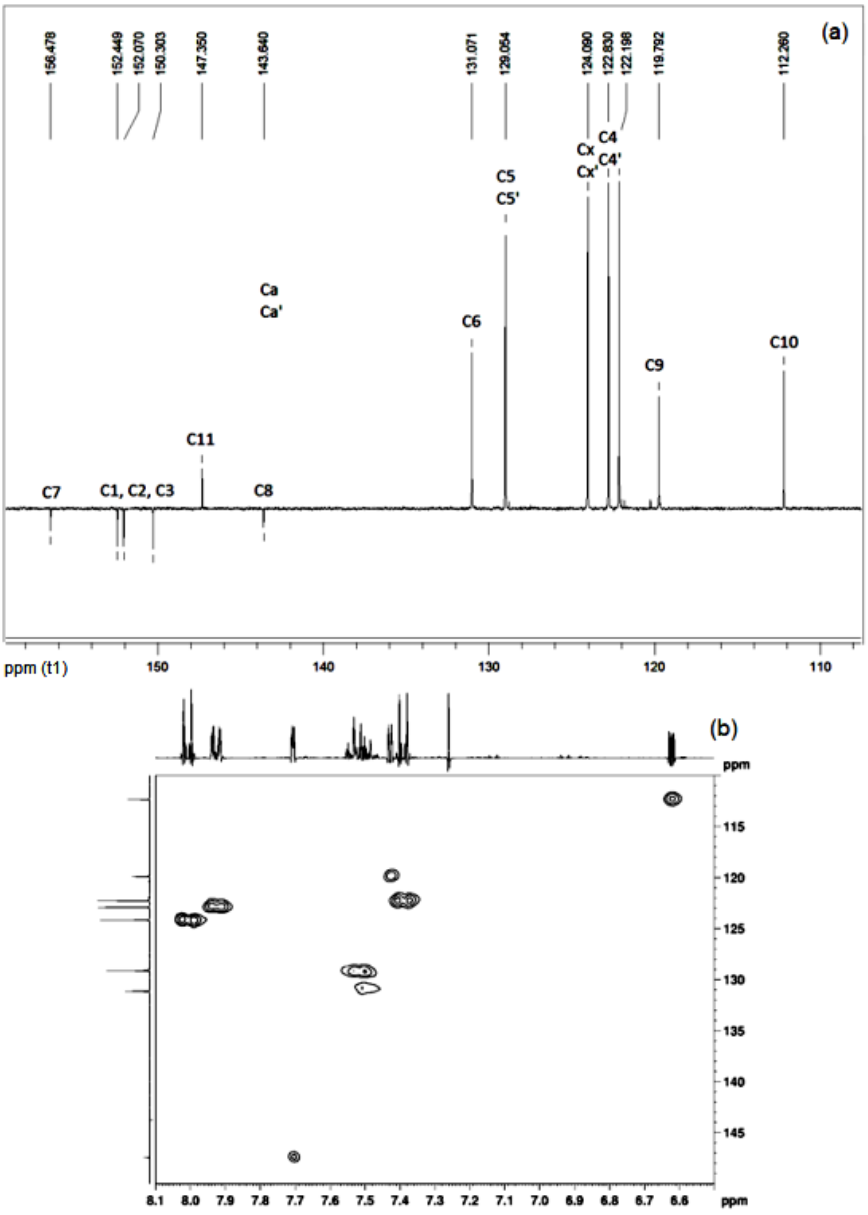

Figure 3. (a) ^{13}C NMR spectrum of PPF; (b) ^{1}H - ^{13}C correlation spectrum of PPF.

Table 1. ^{1}H and ^{13}C NMR parameters of PPF

^{1}H		^{13}C	
Atom	δ (ppm) and coupling constants	Atom	δ (ppm)
-	-	C_1	152.07 *
-	-	C_2	150.30 *
-	-	C_3	152.45 *
H_4 and $H_{4'}$	7.92	C_4 and $C_{4'}$	122.83
H_5 and $H_{5'}$	7.54	C_5 and $C_{5'}$	129.05
H_6	7.48	C_6	131.07
-	-	C_7	156.48
-	-	C_8	143.64
H_9	7.43 ($^{3}J_{H9-H10}$=3.5 Hz; $^{3}J_{H9-H11}$=0.8 Hz)	C_9	119.79
H_{10}	6.62 ($^{3}J_{H10-H9}$=3.5 Hz; $^{3}J_{H10-H11}$=1.7 Hz)	C_{10}	112.26
H_{11}	7.70 ($^{3}J_{H11-H10}$=1.7 Hz; $^{3}J_{H11-H9}$=0.8 Hz)	C_{11}	147.35
H_a and $H_{a'}$	7.39	C_a and $C_{a'}$	122.20
H_x and $H_{x'}$	8.01	C_x and $C_{x'}$	124.09

* These assignments may be interchanged.

3.2. Study on corrosion inhibition of carbon steel in saline water in presence of PPF

3.2.1. Potentiodynamic polarization

Potentiodynamic anodic and cathodic polarization scans were carried out in SW blank and in SW containing different concentrations of PPF: 0.04 mmol L^{-1}; 0.06 mmol L^{-1}; 0.08 mmol L^{-1}; 0.1 mmol L^{-1} (Fig. 4a). From Fig. 4a it can be seen that, in the presence of PPF, the curves are shifted to lower current regions and to higher anodic potential areas, showing the inhibition property of this dye.

Iron oxidation is suppressed by PPF more strongly than the cathodic process is stimulated and the corrosion potential (E_{corr}) becomes higher, with an increase in PPF concentration (Fig. 4a). This result suggests that the addition of this dye in SW disturbs the cathodic reactions and reduces the anodic dissolution of iron. Moreover, Fig. 4a shows that cathodic polarization curves give rise to Tafel lines, indicating that the reactions of all cathodically reduced components, such as hydrogen evolution and oxygen reduction, are activation-controlled [30]. The anodic curves show that the inhibition process depends upon electrode potential. Indeed, for an overall voltage higher than -215 mV vs. $Ag/AgCl_{sat}$, the presence of PPF does not modify the *E*- log*i* curves, which indicates that the dissolution process dominates the inhibition [30]. Therefore, in the vicinity of corrosion potential (E_{corr}), a decrease in the current density is observed starting with the PPF concentration of 0.04 mmol L^{-1}. This phenomenon reflects the formation of an anodic protective film on the electrode surface [30], *via* PPF adsorption on the substrate. The above mentioned changes are more significant with the increase of PPF concentration. These modifications are associated with the decrease of corrosion

current, and consequently, with inhibition efficiency (*IE*) increase. Based on these results, we concluded that: (i) PPF acts as a corrosion inhibitor in SW by suppressing simultaneously the cathodic and anodic processes with anodic predominance; (ii) the organic film formed on electrode surface is stable until the potential value of -215 mV; (iii) above this potential, PPF partial desorption is possible.

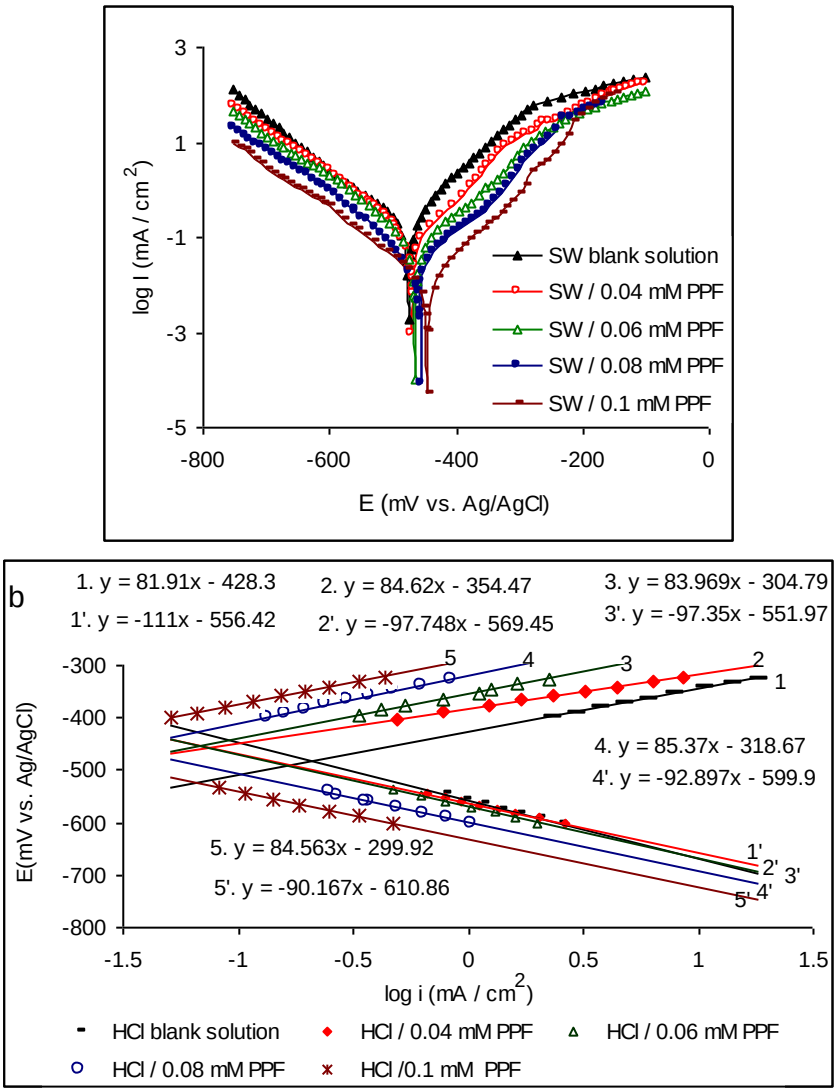

Figure 4. Potentiodinamic curves (a) and Tafel diagram (b) of carbon steel corroded in saline water (SW) without and with various concentrations of PPF, at room temperature.

The corrosion current density (i_{corr}) was calculated at intercept of the anodic and cathodic Tafel lines to corrosion potential, using VoltaMaster 4 software. The Tafel diagram is presented in Fig. 4b. The characteristic equations of anodic and cathodic Tafel lines are inserted in the graph from Fig.4b. The electrochemical parameters such as: corrosion potential (E_{corr}), corrosion current density (i_{corr}), anodic and cathodic Tafel slopes (b_a & b_c) derived from polarization curves and corresponding inhibition efficiency (*EI*) values at different PPF concentrations are given in Table 2. The inhibition efficiency percentage (*IE*) of PPF was determined from polarization measurements according to the following equation, Eq. 1 [31,32]:

$$IE = \frac{i^{0}_{corr} - i_{corr}}{i^{0}_{corr}} \times 100 \qquad (1)$$

where i^0_{corr} and i_{corr} are the corrosion current densities of carbon steel in SW without and with PPF, respectively.

The results showed that the inhibition efficiency increases with increasing PPF concentration, reaching a maximum value of 92.6 % at 0.1 mmol L^{-1} of PPF. Moreover, the slopes of the anodic and cathodic Tafel lines (b_a & b_c) were slightly altered by increasing the tested compound concentration (Table 2). The small change may be due to surface blockage by PPF. This could be attributed to the fact that the anodic carbon steel dissolution and cathodic reactions were both inhibited by this dye through merely blocking the reaction sites of carbon steel surface, without affecting the anodic and cathodic reaction mechanism [33].

3.2.2. Adsorption isotherm

To express the adsorption quantitatively, different adsorption isotherms may be applied. These isotherms characterize the metal/inhibitor/environment system and fit the degree of surface coverage (θ) values. In our study, the best fit was found to obey Temkin adsorption isotherm which may be expressed by Eq. 2 [34]:

$$exp\,(f \cdot \theta) = KC \qquad (2)$$

Equation 2 may be written as the following expression, Eq.3:

$$\theta = \frac{2.303}{f} \cdot logK + \frac{2.303}{f} \cdot logC \qquad (3)$$

where C is the concentration (mol.L^{-1}) of the inhibitor in the bulk electrolyte, θ is the degree of surface coverage *(θ = IE/100)*, K is the adsorption equilibrium constant and f is the number of surface active sites occupied by one inhibitor molecule.

The plot of θ against *logC* for the PPF is given in Fig. 5. The straight line relationship was obtained suggesting the validity of Temkin model for the adsorption of PPF on carbon steel surface, under the simulated laboratory conditions. The equation and deviation from linearity (R^2) are inserted in the graph presented in Fig. 5. The R^2 value is very close to unity, which indicates a strong adherence of the assumption of Temkin adsorption isotherm to experimental data. The slope of this line equals 2.303/f and the intercept is [(2.303/f)·log K], from which the value of K was calculated. It can be observed that K has a value of 513105 L mol^{-1} and f = 4.24. It is noticed that the value of "f" is more than unity. This means that PPF molecules will form a monolayer on the steel surface [35].

The equilibrium constant of adsorption K obtained from the intercepts of Temkin adsorption isotherm is related to the free energy of adsorption (ΔG^0_{ads}) as follows, Eq.4 [35]:

$$K = \frac{1}{55.5} exp\left(-\frac{\Delta G^0_{ads}}{R \cdot T} \right) \quad (4)$$

where R is the universal gas constant, T is the temperature (K) and 55.5 is the molar concentration of water in the solution. The negative value (-42.5 kJ mol^{-1}) obtained for $\Delta G_{ads}{}^{0}$ suggests that the inhibitor's molecules are adsorbed on carbon steel surface. Moreover, this value indicates a spontaneous adsorption of PPF molecules and usually characterizes their strong interaction with the metal surface [34-37]. The value of $\Delta G_{ads}{}^{0}$ of (-40 kJ mol^{-1}) is usually accepted as a threshold value between chemosorption and physical adsorption [37]. The value of $\Delta G_{ads}{}^{0}$ obtained in our study (-42.5 kJ mol^{-1}) indicates a chemical adsorption mechanism.

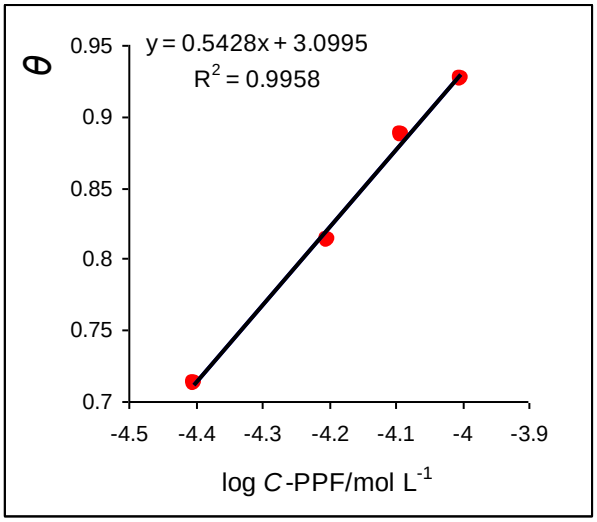

Figure 5. Temkin adsorption plots of carbon steel corroded in saline water (SW) without and with various concentrations of PPF, at room temperature.

3.2.3. Electrochemical impedance spectroscopy (EIS)

Figs. 6a and 6b show the Nyquist and Bode plots for carbon steel in SW without and with PPF; it can be seen that the impedance response of carbon steel in SW shows a significant change after PPF addition (Fig. 6b). This indicates that the carbon steel impedance increases with increasing the inhibitor concentration and, consequently, the inhibition efficiency increases. From Fig.6a it can be seen that Nyquist curves are consisted in one capacitive loop, corresponding to one phase angle maximum in Bode diagram (Fig. 6b).

The equivalent circuit which fits well the experimental data, includes the following elements: the solution resistance (R_s) of the bulk electrolyte, the double layer capacitance (C_{dl}) of the electrolyte at the metal surface and the charge-transfer resistance (R_{ct}) of the metal [30], which is placed in parallel with C_{dl}. The intersection of the capacitive loop with the real axis represents the charge transfer resistance, R_{ct}, at very low frequencies and the electrolytic resistance, R_s, at very high

frequencies which enclosed between the working electrode and the reference one [30]. The double layer capacitance, C_{dl}, was derived from frequency, at which the imaginary component of the impedance ($-Z_{imax}$) was maximal [35,38] using the relationship, Eq. 5 [35,38]:

$$f(-Z_{i\max}) = \frac{1}{2\pi C_{dl} R_{ct}} \qquad (5)$$

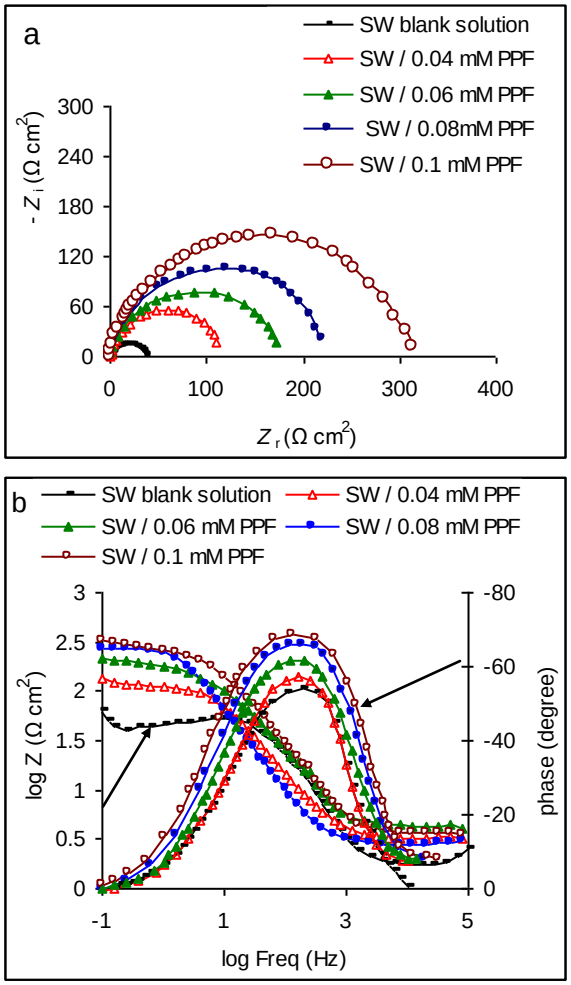

Figure 6. (a) Nyquist plots and (b) Bode plots for carbon steel corroded in saline water (SW) without and with various concentrations of PPF after immersion time of 30 minutes, at room temperature.

More pronounced frequency arcs were obtained for the samples which were immersed in SW containing various concentrations of PPF. This behaviour is usually assigned to changes in density and composition of the substrate layer. It is clear that PPF presence produced a higher charge-transfer resistance (R_{ct}) value, which is interpreted in terms of formation of an effective protective layer that diminishes the corrosion processes.

The impedance parameters derived from EIS measurements R_s, R_{ct}, C_{dl} were calculated using VoltaMaster 4 software with an error of ±1 %, and are listed in Table 2.

Table 2. Electrochemical parameters and inhibition efficiency (*IE*) obtained from potentiodynamic polarization and EIS for carbon steel corroded in SW without and with different concentrations of PPF, at room temperature

Electrochemical results									
C-PPF/ mmol L^{-1}	From potentiodynamic polarization					From EIS			
	E_{corr}/mV vs.Ag/AgCl	i_{corr}/ mA cm^{-2}	b_a/ mV dec^{-1}	$b_{c/}$ mV dec^{-1}	*IE*/ %	R_s/ Ω cm^2	C_{dl}/ μF cm^{-2}	$R_{ct/}$ Ω cm^2	*IE*/ %
0	-482	0.23	81.9	111	0	1.16	259.7	34.6	0
0.04	-474	0.066	84.6	97.7	71.3	1.01	135.8	118.3	70.7
0.06	-469	0.043	83.9	97.3	81.3	0.85	91.8	176.3	80.4
0.08	-458	0.026	85.3	92.9	88.7	0.4	69.6	237.8	85.4
0.1	-449	0.017	84.5	90.1	92.6	0.37	49.9	318.8	89.2

EIS results show that R_s and C_{dl} decrease and R_{ct} increases suggesting that the amount of adsorbed inhibitor molecules increases. This decrease in C_{dl} could be attributed to the decrease in local dielectric constant and/or an increase in the thickness of the electrical double layer [39,40], signifying that PPF acts by adsorption at the interface of metal/solution. The inhibition efficiency (*IE*) was determined using the following relationship, Eq. 6 [31,35]:

$$IE = \left(\frac{R_{ct} - R_{ct}^0}{R_{ct}} \right) \cdot 100 \qquad (6)$$

where R_{ct} and R_{ct}^0 represent the charge-transfer resistances in the presence and absence of PPF.

Inspection of the data in Table 2 reveals that the addition of PPS in saline water increases R_{ct} and decreases C_{dl}, and consequently enhances *IE* reaching a value of 89.2% at 0.1 mmol L^{-1} PPF. It can be seen that the values of inhibition efficiency obtained from potentiodynamic polarization and EIS measurements are in good agreement.

3.2.4. Surfaces characterization. XPS analysis

The samples corroded in SW blank and SW containing 0.1 mmol L^{-1} PPF, after potentiodynamic polarization, were also examined using XPS surface analysis.

Survey spectrum (recorded in a 1200 eV window) of carbon steel surface corroded in SW containing 0.1 mmol L^{-1} PPF shows peaks at 285 eV, 532 eV and 710 eV binding energy corresponding to C(1s) (attributed to adventitious C characteristic line and C from PPF molecule), O(1s) and Fe($2p^{3/2}$) lines. The peaks at 400 eV, 199.5 eV and 1072.3 eV correspond to N(1s) (from PPF molecule), Cl(2p) and Na(1s) lines, respectively (contamination which resulted from the sample being exposed to electrolyte).

Fig. 7a shows the high resolution of XPS spectrum for the Fe($2p^{3/2}$) region of carbon steel corroded in SW containing 0.1 mmol L^{-1}. A similar spectrum was obtained for carbon steel corroded in

SW blank solution. The binding energies for the peaks have been referenced to C-C bond at 285 eV. Metallic iron appeared at 706.6 eV and $Fe^{3+}(2p^{3/2})$ appeared at 710.6 eV and 712.3 eV. The positions and energy values are very close to those observed either for α, γ -FeO(OH) and for Fe_2O_3 structures, respectively [41]. In order to differentiate between FeO(OH) and Fe_2O_3, we have also monitored the O(1s) region (Figs. 7b and 7c).

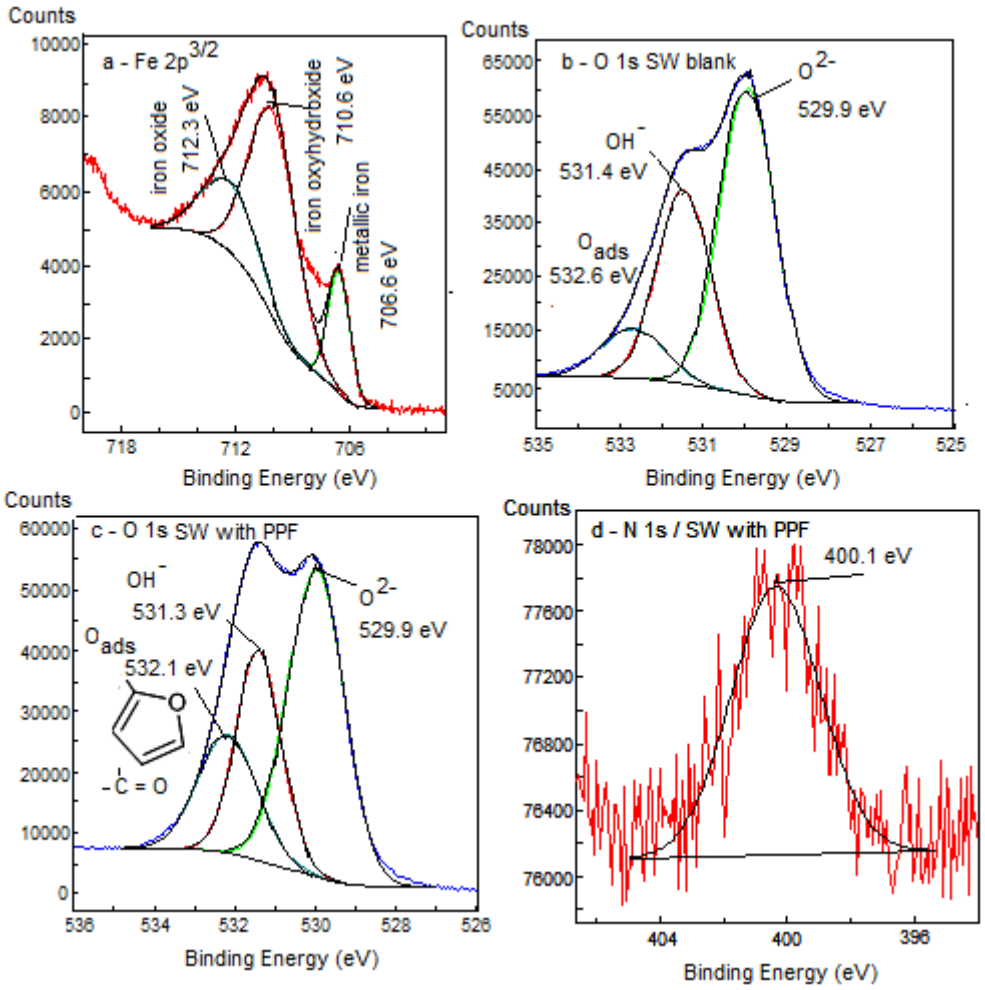

Figure 7. XPS spectra of carbon steel corroded in saline water (SW): a- iron spectrum for carbon steel corroded in SW containing 0.1 mmol L^{-1} PPF; b- O(1s) spectrum for carbon steel corroded in SW blank solution; c- O(1s) spectrum for carbon steel corroded in SW containing 0.1 mmol L^{-1} PPF; d- N(1s) spectrum for carbon steel corroded in SW containing 0.1 mmol L^{-1} PPF.

For the oxygen peak of both samples: corroded in SW blank solution and in SW containing 0.1 mmol L^{-1} PPF, three well resolved peaks were observed in each case, at: 529.9, 531.4, 532.6 eV (Fig. 7b) and 529.9, 531.3, 532.1 eV (Fig. 7c) related to metal oxide, hydroxides [42] and C = O bonds [43] or other adsorbed species such as oxygen from water [41]. For α - FeO(OH) or/and γ - FeO(OH) two well resolved peaks were observed at 529.9 eV (O^{-2}) and 531.4/531.1 eV (OH^-). The O(1s) peak for Fe_2O_3 was found at 530.1 eV and 529.9 eV, respectively. It can be noticed that, in presence of PPF (Fig. 7c), the adsorbed species amount is larger than in absence of PPF (Fig. 7b), related to –O-CO- group and oxygen atom from furanic ring. Oxide-hydroxides of iron may occur in anhydrous

[FeO(OH)] or hydrated [$FeO(OH)\cdot nH_2O$] forms. The monohydrate [$FeO(OH)\cdot H_2O$] might otherwise be described as iron (III) hydroxide [$Fe(OH)_3$], and is also known as hydrated iron oxide or yellow iron oxide.

Further relevant information about the surface chemistry of the carbon steel corroded in SW containing 0.1 mmol L^{-1} PPF is obtained from the XPS spectral analysis of N(1s) photo-peak (Fig. 7d). The spectral simulation of the N(1s) photo-peak (Fig. 7d) for carbon steel corroded in presence of PPF shows organic nitrogen species at 400.1 eV such as amine, amide, imine, etc [44,45]. Indeed, this binding energy corresponds to C-N bonds from PPF molecule.

Taking these data into account, we may conclude that: (i) XPS demonstrates the presence of a superficial layer on the corroded carbon steel surface in SW blank solution, confirming the formation of a product, as a result of corrosion action. At this stage, it was showed that the main product of corrosion is formed of Fe^{3+} species which are similar to those shown by Fe^{3+} oxide/oxyhydroxide consisting of Fe_2O_3 and α-FeOOH and/or γ-FeOOH, α-FeOOH/γ-FeOOH and $Fe(OH)_3$, where oxyhydroxides are the main phase; (ii) in the presence of PPF, the protective layer consists of a thin organic film and an amount of the iron compounds already described above; (iii) the survey spectrum shows that this layer can incorporate Cl^- and Na^+ ions; (iv) the presence of nitrogen and oxygen atoms, as active centres in PPF molecule can enhance the binding between carbon steel surface and this azo ester, which consequently results in the formation of a compact and impermeable layer. We assume that PPF molecules are adsorbed on the metal surface through interactions between the metal and the lone pairs of electrons of: (a) nitrogen from the azo group (-N=N-) and (b) oxygen from–O-CO- group and, more probably, from the furanic ring.

3.2.5. Adsorption mechanism

Theoretical chemistry has been used to explain the mechanism of corrosion inhibition. Parameterized Model number 3 (PM3) semiempirical method was successfully used to predict the electron density distribution inside of PPF molecule. The optimized geometry (Fig.8a) and the maps (2D and 3D) of electron density distribution of the studied azo dye (PPF) are given in Fig.8.

Figs.8b and 8c reveal that the highest levels of electron density are found in the vicinity of the oxygen atoms attached to carbon atom from –O-CO- group, in vicinity of the oxygen atom from the furanic ring and in vicinity of nitrogen atoms from the azo group. Moreover, lowest levels of electron density are found in the inside of aromatic and furanic rings. Therefore, our prognosis is that this azo dye can be adsorbed on the carbon steel surface using these active centers: (i) nitrogen atoms from the azo group (-N=N-); (ii) oxygen from furanic ring; (iii) oxygen atoms attached to carbon from –O-CO- group. This hypothesis is in good agreement with XPS results.

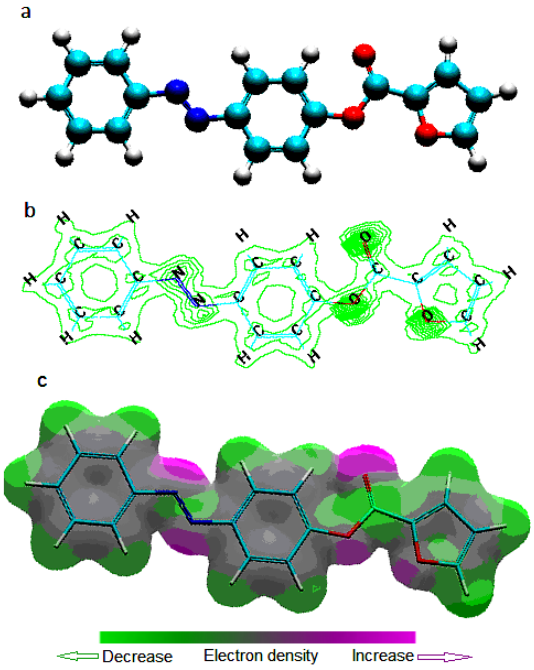

Figure 8. The optimized geometry (a); total electron density surface: 2D map (b) and 3D map (c) for PPF (the electron rich regions are violet and the electron poor regions are green).

4. CONCLUSIONS

4-(phenyldiazenyl)phenyl 2-furoate is a novel dye obtained by reacting 4-(phenyldiazenyl)phenol with 2-furoyl chloride in pyridine. The structure of this new compound has been assigned using ^{1}H and ^{13}C NMR, mass spectrometry and elemental analysis.

PPF behaves as a corrosion inhibitor of carbon steel in saline water. In SW, at 0.1 mmol L^{-1}, it has an inhibition efficiency of 91 ± 1 % obtained from potentiodynamic polarization and electrochemical impedance spectroscopy. PPF acts as adsorption inhibitor on carbon steel surface; adsorption is spontaneous and is best described by Temkin isotherm.

In the presence of PPF, XPS analysis confirmed the existence of a superficial layer providing a good corrosion protection of the electrodes. XPS analysis confirms the adsorption of PPF on carbon steel surface; at this stage, the main product of corrosion is a non-stoichiometric Fe^{3+} oxide/oxyhydroxide, consisting of a mixture of α, γ-FeOOH, $Fe(OH)_3$ and Fe_2O_3, where oxyhydroxides represent the main phase.

PM3 method was successfully used to predict the electron density distribution inside of PPF molecule. Thus, PPF can be adsorbed on the carbon steel surface through interactions between the metal and the lone pairs of electrons of nitrogen atoms from the azo group (-N=N-), oxygen from–O-CO- group and oxygen atom from the furanic ring. The adsorption layer functions as a barrier isolating the metal from the corrosion.

References

1. K. Venkataraman, *The chemistry of synthetic dyes,* New-York and London: Academic Press (1970).
2. M. Gür, H. Kocaokutgen and M. Taş, *Dyes Pigments,* 72 (2007) 101.
3. J. Griffiths, *Colour and constitution of organic molecules,* New-York and London: Academic Press(1976).
4. P. Gregory, *High-technology applications of organic colorants,* Plenum Press, New-York and London: Plenum Press (1991).
5. B.H. Hameed, A.L. Ahmad and K.N.A. Latiff, *Dyes Pigments,* 75 (2007) 143.
6. E. Lorenc-Grabowska, G. Gryglewicz, *Dyes Pigments,* 74 (2007) 34.
7. M. Doğan, Y. Özdemir and M. Alkan, *Dyes Pigments,* 75 (2007) 701.
8. S. Merah, L. Larabi, O. Benali and Y. Harek, *Pigm. Res. Tech.,* 37 (2008) 291.
9. O. Benali, L. Larabi, S. Merah and Y. Harek, *J. Mater. Environ. Sci.,* 2 (2011) 39.
10. M. Abdel, N.P. Ahmadi and R.A. Khosroshahi, J. Sol. State Electrochem. 14 (2010) 1317.
11. E.E. Ebenso and E.E. Oguzie, EE. *Mater. Lett.,* 59 (2005) 2163.
12. A. Ashassi-Sorkhabi, B. Masoumi, P. Ejbari and E. Asghari, *J. Appl. Electrochem.,* 39 (2009)1497.
13. E.E. Oguzie, G.N. Onuoha and A.I. Onuchukwu, *Mater. Chem. Phys.,* 89 (2005) 305.
14. E.E. Oguzie and E.E. Ebenso, *Pigm. Res. Tech.,* 35 (2006) 30.
15. L. Tang L, G. Mu and G. Liu, *Corros. Sci.,* 45 (2003) 2251.
16. H. Ashassi-Sorkhabi, E. Asghari and P. Ejbari, *Acta Chim. Slov.,* 58 (2011) 270.
17. Zarrouk , B. Hammouti , H. Zarrok , M. Bouachrine , K.F. Khaled and S.S. Al-Deyab, *Int. J. Electrochem. Sci.,* 7 (2012) 89.
18. A. Samide, I. Bibicu, M.S. Rogalski and M. Preda, *Corros. Sci.,* 47 (2005) 1119.
19. A. Samide and I. Bibicu, *Surf. Interface Anal.,* 40 (2008) 944.
20. A. Samide, I. Bibicu, M. Agiu and M. Preda, *Mater. Lett.,* 62 (2008) 320.
21. A. Samide, I. Bibicu and E. Turcanu, *Chem. Eng. Commun.,* 196 (2009) 1008.
22. A. Moanta, C. Ionescu, P. Rotaru, M. Socaciu and A. Harabor, *J. Therm. Anal. Calorim.,* 102 (2010) 1079.
23. A. Rotaru, A. Moanta, G. Popa, P. Rotaru and E. Segal, *J. Therm. Anal. Calorim.,* 96 (2009) 485.
24. A. Rotaru A. Moanta, P. Rotaru and E. Segal, *J. Therm. Anal. Calorim.,* 95 (2009) 161.
25. A. Rotaru, A. Kropidłowska, A. Moanta, P. Rotaru and E. Segal, *J. Therm. Anal. Calorim.,* 92 (2008) 233.
26. A. Rotaru, A. Moanta, A. Sălăgeanu, P. Budrugeac and E. Segal, *J. Therm. Anal. Calorim.,* 87 (2007) 395.
27. A. Moanţă, B. Tutunaru, P. Rotaru, *J. Therm. Anal. Calorim.,* DOI: 10.1007/s10973-012-2416-1, 2012.
28. E. Pretsch, P. Bühlmann and M. Badertscher, *Structure determination of organic compounds:Tables of spectral data,* 4th ed. Berlin: Springer-Verlag (2009).
29. D.F. Ewing, *Org. Magn. Reson.,* 12 (1979) 499.
30. B. Zerga, A. Attayibat, M. Sfaira, M. Taleb, B. Hammouti, M. Ebn Touhami, S. Radi, Z. Rais, *J. Appl. Electrochem.,* 40 (2010) 1575.
31. Y. H. Ahmad, A. S. Mogoda, A. G. Gadallh, *Int. J. Electrochem. Sci.,* 7 (2012) 4929.
32. El-Mehdi, B. Mernari, M. Traisnael, F. Bentiss, M. Lagrenee, *Mater. Chem. Phys*., 77 (2002) 489.
33. K. F. Khaled, N. Hackerman, *Electrochim. Acta*, 48 (2003) 2715.
34. B. Zerga, B. Hammouti, M. Ebn Touhami, R. Touir, M. Taleb, M. Sfaira, M. Bennajeh, I. Forssal, *Int. J. Electrochem. Sci.,* 7 (2012) 471.
35. A. S. Fouda, H. A. Mostafa, H. M. El-Abbasy, *J. Appl. Electrochem.,* 40 (2010) 163.
36. M. A. Migahed, *Mater. Chem. Phy*. 93 (2005) 48.

37. H. Zarrok, S. S. Al-Deyab, A. Zarrouk, R. Salghi, B. Hammouti, H. Oudda, M. Bouachrine, F. Bentiss, *Int. J. Electrochem. Sci.,* 7 (2012) 4047.
38. L. Bammou, M. Mihit, R. Salghi, A. Bouyanzer, S.S. Al-Deyab, L. Bazzi, B. Hammouti, *Int. J. Electrochem. Sci.,* 6 (2011) 1454.
39. W. Stephen Tait, *An Introduction to Electrochemical Corrosion Testing for Practicing Engineers and Scientists,* Pair O Docs Publications (1994).
40. S. Muralidharan, K. L. N. Phani, S. Pitchumani, S. Ravichandran, S. V. K. Iyer, Polyamino-Benzoquinone, *J. Electrochem. Soc.* 142 (1995) 1478.
41. A.P. Grosvenor, B.A. Kobe, M.C. Biesinger and N.S. McIntyre, *Surf. Interface Anal.,* 36 (2004)1564.
42. J.C. Dupin, D. Gonbeau, P. Vinatier and A. Levasseur, *Phys. Chem. Chem. Phys.,* 2 (2002) 1319.
43. Z.A. Yi, Y.Y. Xu, L.P. Zhu, H.B. Dong and B.K. Zhu, *Chin. J. Polym. Sci.,* 27 (2009) 695.
44. M. Vinnichenko, T. Chevolleau, M.T. Pham, L. Poperenko and M.F. Maitz, *Appl. Surf. Sci.,* 201 (2002) 41.
45. G. Billon, E. Ouddane, L. Gengembre and A. Boughriet, *Phys. Chem. Chem. Phys.*, 4 (2002) 751.